Rashba-like spin degeneracy breaking in coupled thermal antenna lattices

Kobi Frischwasser, Igor Yulevich, Vladimir Kleiner, and Erez Hasman*

Micro and Nanooptics Laboratory, Faculty of Mechanical Engineering, and Russell Berrie Nanotechnology Institute, Technion - Israel Institute of Technology, Haifa 32000, Israel
mehasman@technion.ac.il

Abstract: Observation of a spin degeneracy breaking in thermal radiation emitted from an inhomogeneous anisotropic lattice composed of coupled antennas supporting surface waves is presented. The spin degeneracy removal is manifested by a spin-dependent momentum splitting of the radiative mode which resembles the Rashba effect. The spin split dispersion arises from the inversion asymmetry of the lattice. Our experiment confirms that the spatial rate of the inhomogeneity determines the degree of the spin-dependent momentum redirection. The influence of the inversion asymmetry on the dispersion was studied by comparing the results to those produced by homogeneous lattices and characterizing the behavior of the isolated thermal antennas.

References and links

1. P. Zeeman, "On the influence of Magnetism on the Nature of the Light emitted by a Substance," Philos. Mag. **43**, 226–239 (1897).
2. E. I. Rashba, "Properties of semiconductors with an extremum loop. 1. Cyclotron and combinational resonance in a magnetic field perpendicular to the plane of the loop," Sov. Phys. Solid State **2**, 1109 (1960).
3. K. Ishizaka, M. S. Bahramy, H. Murakawa, M. Sakano, T. Shimojima, T. Sonobe, K. Koizumi, S. Shin, H. Miyahara, A. Kimura, K. Miyamoto, T. Okuda, H. Namatame, M. Taniguchi, R. Arita, N. Nagaosa, K. Kobayashi, Y. Murakami, R. Kumai, Y. Kaneko, Y. Onose, and Y. Tokura, "Giant Rashba-type spin splitting in bulk BiTeI," Nat. Mater. **10**(7), 521–526 (2011).
4. G. Dresselhaus, "Spin–orbit coupling effects in zinc blende structures," Phys. Rev. **100**(2), 580–586 (1955).
5. R. A. Beth, "Mechanical Detection and Measurement of the Angular Momentum of Light," Phys. Rev. **50**(2), 115–125 (1936).
6. O. Hosten and P. Kwiat, "Observation of the spin hall effect of light via weak measurements," Science **319**(5864), 787–790 (2008).
7. K. Y. Bliokh, A. Niv, V. Kleiner, and E. Hasman, "Geometrodynamics of spinning light," Nat. Photonics **2**(12), 748–753 (2008).
8. K. Y. Bliokh, "Geometrodynamics of polarized light: Berry phase and spin Hall effect in a gradient-index medium," J. Opt. A. **11**, 094009 (2009).
9. Y. Gorodetski, S. Nechayev, V. Kleiner, and E. Hasman, "Plasmonic Aharonov-Bohm effect: Optical spin as the magnetic flux parameter," Phys. Rev. B **82**(12), 125433 (2010).
10. Y. Gorodetski, N. Shitrit, I. Bretner, V. Kleiner, and E. Hasman, "Observation of optical spin symmetry breaking in nanoapertures," Nano Lett. **9**(8), 3016–3019 (2009).
11. Y. Gorodetski, A. Niv, V. Kleiner, and E. Hasman, "Observation of the spin-based plasmonic effect in nanoscale structures," Phys. Rev. Lett. **101**(4), 043903 (2008).
12. N. Dahan, Y. Gorodetski, K. Frischwasser, V. Kleiner, and E. Hasman, "Geometric doppler effect: spin-split dispersion of thermal radiation," Phys. Rev. Lett. **105**(13), 136402 (2010).
13. J.-J. Greffet, R. Carminati, K. Joulain, J.-P. Mulet, S. Mainguy, and Y. Chen, "Coherent emission of light by thermal sources," Nature **416**(6876), 61–64 (2002).
14. E. D. Palik, *Handbook of Optical Constants of Solids* (Academic, Orlando, 1985).
15. J. A. Schuller, T. Taubner, and M. L. Brongersma, "Optical antenna thermal emitters," Nat. Photonics **3**(11), 658–661 (2009).
16. T. W. Ebbesen, H. J. Lezec, H. F. Ghaemi, T. Thio, and P. A. Wolff, "Extraordinary Optical Transmission through Sub-Wavelength Hole Arrays," Nature **391**(6668), 667–669 (1998).
17. C. F. Bohren and D. R. Huffman, *Absorption and Scattering of Light by Small Particles* (Wiley-VCH, 2004).

18. K. D. Ko and C. K. Toussaint, Jr., "A simple GUI for modeling the optical properties of single metal nanoparticles," J. Quant. Spectrosc. Radiat. Transf. **110**(12), 1037–1043 (2009).
19. D. H. Goldstein, *Polarized Light,* (CRC Press, 2011).
20. N. Shitrit, I. Bretner, Y. Gorodetski, V. Kleiner, and E. Hasman, "Optical spin Hall effects in plasmonic chains," Nano Lett. **11**(5), 2038–2042 (2011).
21. B. C. Hsu and J.-F. S. Van Huele, "Spin dynamics for wave packets in Rashba systems," Phys. Rev. B **80**(23), 235309 (2009).

1. Introduction

The spin state of elementary particles, atoms and molecules plays a key role in fundamental effects in physics. For instance, an external magnetic field causes energy separation of electrons due to the interaction with their spin (Zeeman effect) [1]. Spin-dependent momentum separation of charge carriers (spin-orbit interaction) can occur due to structural inversion asymmetry in bulk materials (Rashba and Dresselhaus effects) [2–4]. These two mechanisms show distinct patterns of energy dispersion, see Fig. 1. The photonic analogy of spin-orbit interaction was recently presented, wherein, the spin of the photons (helicity state) plays the role of the spin of charge carriers where $\sigma_+ = 1$ ($\sigma_- = -1$) stands for right-handed (left-handed) circular polarization, respectively [5]. Spin-dependent deflection of light was obtained for propagation in gradient-index media [6–8] and with the scattering of surface plasmon polaritons (SPPs) from metallic nanostructures [9–11]. Recently, spin-dependent thermal emission from a structure consisting of an inhomogeneous anisotropic coupled antenna array supporting surface phonon polaritons (SPhPs) was observed [12]. Dispersion spin-splitting of thermal radiation occurred due to the interaction of electromagnetic surface waves with a spatially rotating anisotropic structure.
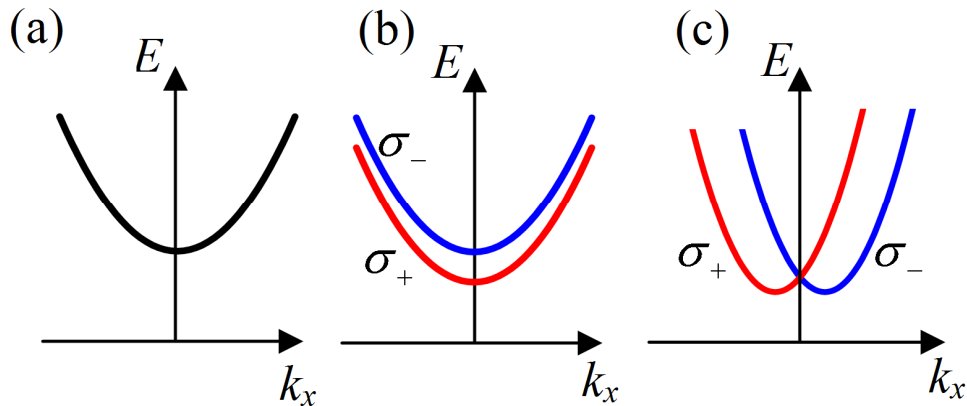
Fig. 1. Energy dispersion schemes of (a) spin-degenerated system, (b) energy splitting of the dispersion associated with Zeeman effect, (c) spin-dependent shift of the dispersion in the momentum space.

Here we investigate the influence of the symmetry of lattices composed of thermal antennas on the emission dispersion. We observed Rashba-like spin split bands of emission from inversion asymmetric structures. The strength of the spin splitting in the momentum was found to be equal to twice the spatial rate of the lattices' inhomogeneity. We found that the spatial rate corresponds to the Rashba parameter (α_R) which determines the momentum offset in the electronic bands [3]. In section 2 of the paper we investigate the dispersion of the thermal emission emerging from a homogeneous lattice composed of isotropic thermal antennas. The measured dispersion is in accordance with the momentum-matching condition of the SPhP modes coupled to radiative modes. Section 3 focuses on the emission properties of the individual anisotropic antennas, observing the local modes. Theoretical calculation

using the modified long wavelength approximation theory (MLWA) shows a good agreement with the measured resonant frequencies of the localized modes. In section 4 we study the behavior of a homogeneous lattice composed of anisotropic antennas. A strong linear polarization perpendicular to the long axis of the antennas was observed for the slow modes at various orientations of the antennas. Section 5 presents experimental results and a theoretical analysis of the emission dispersions for inhomogeneous anisotropic lattices under broken inversion symmetry. Finally, concluding remarks are presented in section 6.

2. Homogeneous isotropic lattice

SPhPs are created due to resonant collective lattice vibrations in the interface of a polar material and a dielectric [13]. An essential condition for excitation of SPhPs is the negative permittivity of the polar material, which is fulfilled for silicon carbide (SiC) at a wide range
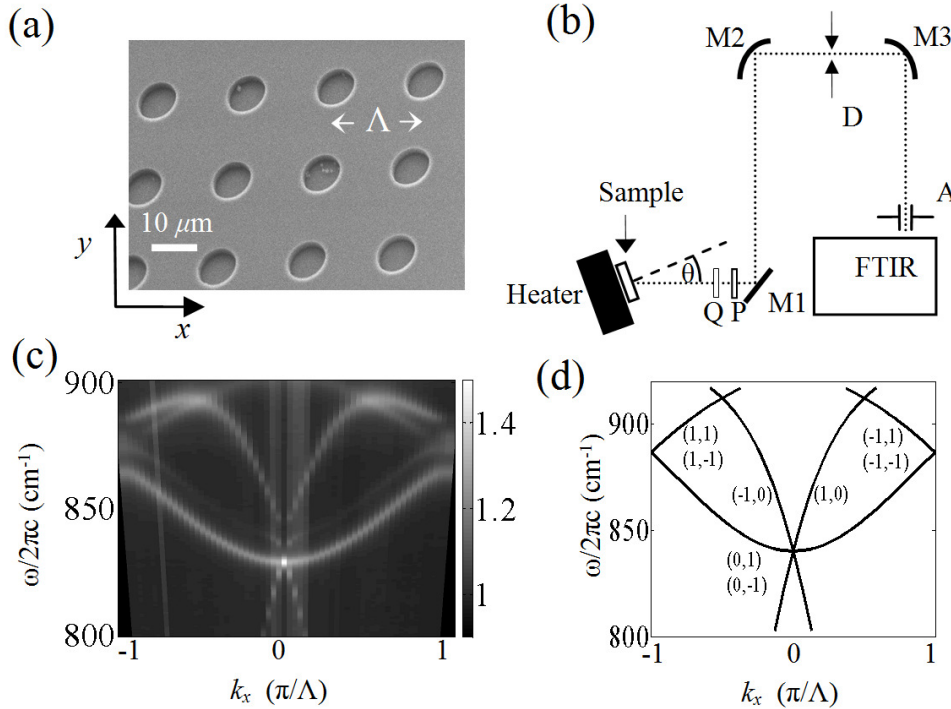
Fig. 2. (a) Scanning electron microscope (SEM) image of the L1 lattice etched on a SiC substrate with a period of $\Lambda = 11.6\,\mu m$, depth $h = 1\,\mu m$ and diameter $d = 4.8\,\mu m$. (b) Experimental set-up used to measure dispersion of the emitted radiation. Q - quarter waveplate, P - polarizer, M1 - flat mirror, M2/M3 - parabolic mirrors (focal length 250mm), D - angular resolution slit in the focal length, A - field of view aperture, diameter equals 8mm. (c) Measured dispersion of thermal emission from the L1 lattice. Color scale – intensity, a.u. (d) The calculated dispersion.

of frequencies above the transverse optical phonon resonance $\omega_{TO}/2\pi c = 793\,cm^{-1}$ [14]. It has been shown that due to their low damping and high density of states, SPhPs dramatically modify the thermal emission properties of the SiC in the mid-infrared regime [12, 13, 15]. The coupling of SPhPs to radiative modes can be achieved by creating periodic corrugations on the surface of the polar material. A *homogeneous isotropic lattice* (L1) consisting of a rectangular array of circular voids upon a 6H-SiC substrate (isotropic 'anti-particles') with a diameter $D = 4.8\mu m$, depth $h = 1\mu m$ and periodicity $\Lambda = 11.6\mu m$, was fabricated using standard photolithographic techniques (see Fig. 2 (a)). Angle-resolved emission spectra were

measuredby a Fourier transform infrared spectrometer (Bruker, Vertex 70) at different polar angles, θ, relative to the normal direction and at zero azimuthal angle (Fig. 2(b,c)), while heating the sample to 773 K. The coupling of SPhPs to radiative modes by periodic corrugations is achieved according to the momentum-matching condition, $k_x \hat{x} = \vec{k}_{SPhP} + iG_x \hat{x} + jG_y \hat{y}$, where, $\left| \vec{k}_{SPhP} \right| = k_0 \left[(\varepsilon_s \varepsilon_a) / (\varepsilon_s + \varepsilon_a) \right]^{\frac{1}{2}}$ [16]. Here, $k_x = k_0 \sin \theta$, k_0 is the wave number of light in free space, ε_s and ε_a are the frequency-dependent relative permittivities of the substrate and the superstrate (in our case $\varepsilon_a = 1$ for air); G_x and G_y are the lattice momenta associated with the periodicity of the array, $G_x = G_y = 2\pi / \Lambda$, and the indices (i, j) denote the specific radiative modes. The calculated modes, using the momentum-matching condition, depicted in Fig. 2(d), exhibit a good agreement with the measured dispersion.

3. Local modes of anisotropic antennas

Next, we replace the isotropic antennas in the homogeneous lattice with anisotropic antennas (rectangular voids with dimensions *1.2μm × 4.8μm*; depth *h = 1μm*, see Fig. 3 (a), right inset).
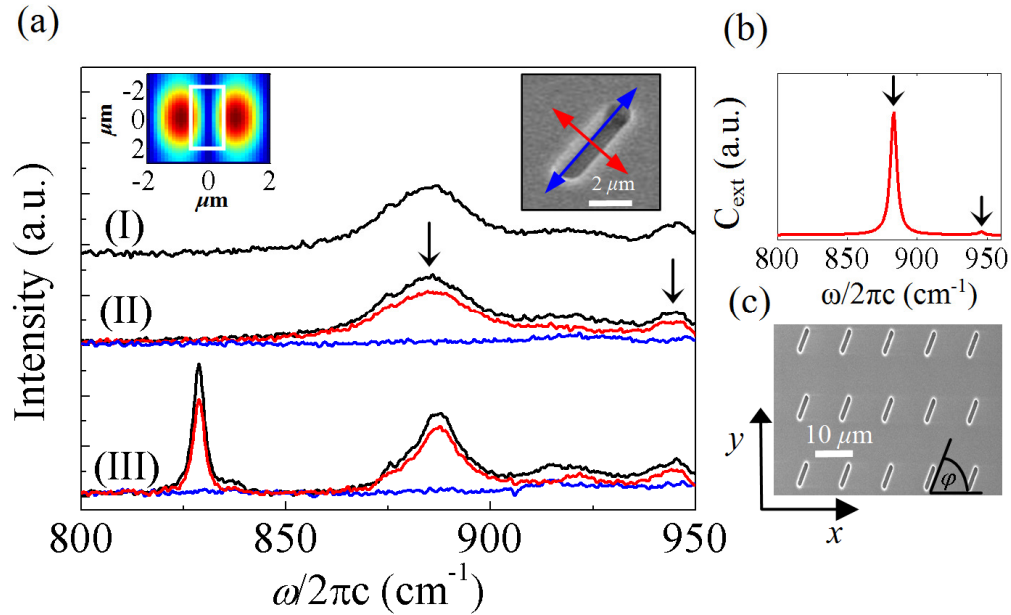
Fig. 3. (a) Spectral emission from the isolated thermal antenna, measured at $\theta = 6°$ (I) and $\theta = 0°$ (II) [SEM image of the antenna, right inset], and for L3 lattice at $\theta = 0°$ (III) [SEM image in (c)]; red and blue curves correspond to polarization along the short axis and long axis of the antenna, respectively, and the black for the total intensity. Left inset presents FDTD simulation of the intensity distribution in vicinity of an isolated antenna at 883.7 cm^{-1}, white square indicates the location of the antenna. Black arrows point to the local resonances. (b) Calculated extinction cross section of an isolated antenna attained for polarization along the short axis of the antenna.

The spectrum and the polarization of the thermal emission from a *homogeneous anisotropicantenna lattice* are fundamentally affected by the local modes of each individual antenna. In order to characterize the thermal emission from the individual antenna, we measured the emission spectrum from an array of *randomly distributed rectangular voids* (L2), thereby eliminating correlation effects due to periodicity. Figure 3(a- I, II) shows two similar spectral cross-sections which were measured at $\theta = 0^o$ and $\theta = 6^o$. Two distinct

resonances, attributable to the local modes at $\omega_1/2\pi c = 885.7\,cm^{-1}$ and $\omega_2/2\pi c = 944.7\,cm^{-1}$, were observed. Note that the resonances are independent of the observation angle, as expected from the behavior of localized modes. The resonances exhibit a strong linear polarization along the direction of the short axis of the antenna, whereas for the emission polarized along the long axis the intensity is negligible. This behavior was confirmed by a finite difference time domain (FDTD) simulation of the local intensity distribution in the vicinity of the antenna, shown in Fig. 3 (a), left inset. Such a polarization dependence characterizes voids at SiC surface - 'anti-particles', while for rectangular particles of SiC surrounded by air, the dominant polarization state is along the long axis of the antenna [15]. The calculation of the antennas' resonant frequencies using the quasi-static (QS) approximation [17] results in a single resonance at $\omega_1^{(QS)}/2\pi c = 950.6\,cm^{-1}$. In order to get a higher order solution, we used the modified long wavelength approximation (MLWA) theory [18] to determine the extinction cross section of elliptically shaped voids embedded in a SiC substrate. The calculated resonant frequencies, $\omega_1^{(MLWA)}/2\pi c = 883.7\,cm^{-1}$ and $\omega_2^{(MLWA)}/2\pi c = 946.1\,cm^{-1}$, are in good agreement with the measured localized modes; see Figs. 3(b) and 3(a-II).

4. Homogeneous anisotropic lattice

A *homogeneous anisotropic lattice* (L3) comprised of a periodic rectangular array of anisotropic thermal antennas that were identically oriented at the angle $\varphi = 60^o$ with respect to the x direction, was then fabricated (see Fig. 3(c)). The measured emission from the structure in the normal direction is shown in Fig. 3(a-III). One can see that in addition to the
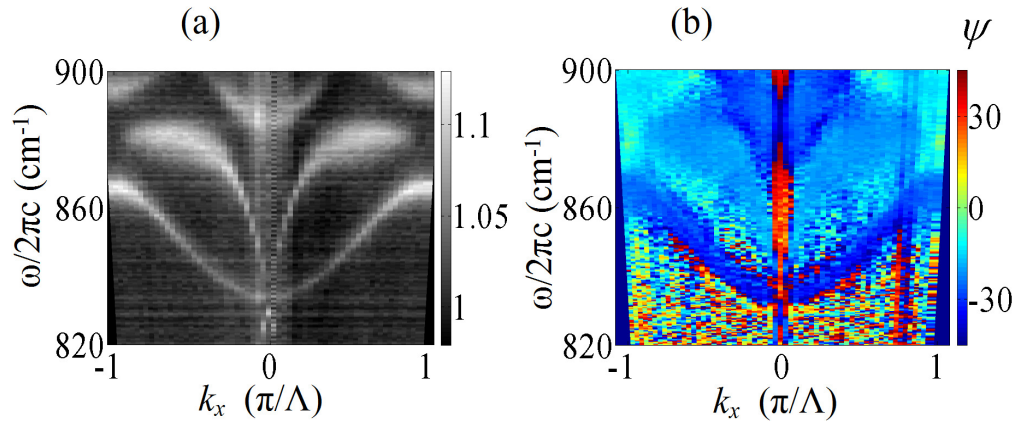
Fig. 4. (a) Measured dispersion of thermal emission from the L3 lattice ($\varphi = 60^o$) Color scale - intensity, a.u. (b) Measured orientation angle of the polarization ellipse, ψ (°), for the dispersion in (a).

localized modes (Fig. 3(a-II)) the spectrum contains a narrow peak of the collective mode at $830\,cm^{-1}$, which is also polarized along the short axis of the antenna. By angle-resolved spectroscopy, we found that this spectral peak corresponds to strongly dispersive modes (Fig. 4(a)) that are similar to the radiative modes of the isotropic antenna array (Fig. 2(c)). A polarization analysis of the dispersion was then performed by measuring the Stokes parameters (S_0, S_1, S_2, S_3) [19] to obtain the orientation angle of the polarization ellipse, ψ, and its ellipticity angle, χ of the emission, using the relations $\tan(2\psi) = S_2/S_1$ and $\sin(2\chi) = S_3/S_0$. For an array with $\varphi = 60^o$, we obtained a typical value of $\chi \approx 0$ for the (0, ±1) modes, which indicates the emission having a strong linear polarization state. The obtained distribution of the angle ψ (see Fig. 4(b)) shows that these modes are polarized along

the short axis of the antenna, $\psi = -30°$. The same measurements were performed for arrays with various orientation angles of the antennas $(\varphi = 0°, 30°, 90°)$, with the results verifying that $\psi = \varphi \pm 90°$. Note that the $(0, \pm 1)$ modes are most affected by the local orientation of the antennas. This can be attributed to the low group velocity of these modes, which enables a strong interaction with the antennas.

5. Inhomogeneous anisotropic lattice: spin split dispersion

In order to study the emission of an *inhomogeneous anisotropic lattice* (L4) we fabricated arrays of rectangular antennas with a period $\Lambda = 11.6 \ \mu m$ whose orientation was sequentially rotated along the *x*-axis, see Fig. 5(a). The antennas' angle with respect to the *x* direction, $\varphi(x) = (\pi / a)x$, changes at a spatial rotation rate of $\Omega = d\varphi(x) / dx = \pi / a$, where a is the distance along the *x* direction for a π rotation. We obtained a spin-projected dispersion (in the k_x momentum direction) for a lattice with $\Omega = 0.17(\pi / \Lambda)$ by measuring the S_3 component of the Stokes vectors, which represents the circular polarization portion within the emitted light (Fig. 5(b)). For the normalized parameter $\hat{S}_3 = S_3 / S_0$, the component values $\hat{S}_3 = \pm 1$ correspond to the pure states of light with spin $\sigma_\pm$. The spin-resolved dispersion of the emitted radiation shows a distinct spin - controlled momentum separation of the $(0, \pm 1)$ modes. We measured the degree of splitting of these modes, $2\Delta k$, for various Ω, (Fig. 5(c)), and found that it grows linearly with Ω, so as $\Delta k = \sigma \Omega$, where σ denotes one of two possible basic spin state of the emitted field (Fig. 5(d)). The observed effect is due to a spin-orbit interaction resulting from the dynamics of the surface waves propagating along the structure whose local anisotropy axis is rotated in space. The spin symmetry breaking is caused by the absence of inversion symmetry in our system. In general, time reversal symmetry (TRS) in a crystal results in energy relation $E(\mathbf{k}, \sigma_+) = E(-\mathbf{k}, \sigma_-)$. If the crystal lattice has inversion symmetry (IS), i.e., the operation $\mathbf{r} \rightarrow -\mathbf{r}$ does not change the crystal lattice, one will obtain $E(\mathbf{k}, \sigma_+) = E(-\mathbf{k}, \sigma_+)$ and $E(\mathbf{k}, \sigma_-) = E(-\mathbf{k}, \sigma_-)$. Consequently, if both TRS and IS are present, the band structure should satisfy the condition $E(\mathbf{k}, \sigma_+) = E(\mathbf{k}, \sigma_-)$. One can see that the inhomogeneous antenna lattice (L4), in our case, has an inversion asymmetry along the *x* direction $\varphi(x) \neq \varphi(-x)$, resulting in $E(k_x, \sigma_+) \neq E(k_x, \sigma_-)$. However, from the dispersion depicted in Fig. 5, it is evident that $E(k_x, \sigma_+) = E(-k_x, \sigma_-)$. Therefore, while our system has TRS, it has broken IS. Such behavior is similar to the Rashba spin splitting in electron bands of heterostructures which stems from inversion asymmetry in the structure [3]. The momentum offset Δk in the Rashba effect is proportional to the Rashba parameter α_R, ($\Delta k = m^* \alpha_R / \hbar^2$, m^* representing the effective mass of electrons), so in our observed photonic effect, the spatial rate of the lattices' inhomogeneity, Ω, resembles $m^* \alpha_R / \hbar^2$. In the same manner, we can define a Rashba-like energy, E_{R-L}, ($E_{R-L} = \hbar \Delta \omega_{R-L}$, see Fig. 5) that is proportional to Ω^2, in accordance with the parabolic band approximately obtained in our case for the slow modes $(0, \pm 1)$. Note that in the Rashba effect with a parabolic band dispersion derived from a two-dimensional electron gas, the Rashba energy is equal to $m^* \alpha_R^2 / 2\hbar^2$, ($E_R = \hbar^2 \Delta k^2 / 2m^*$) [3]. So the characteristic parameters quantifying the spin split effect are the momentum offset and the Rashba-like energy.
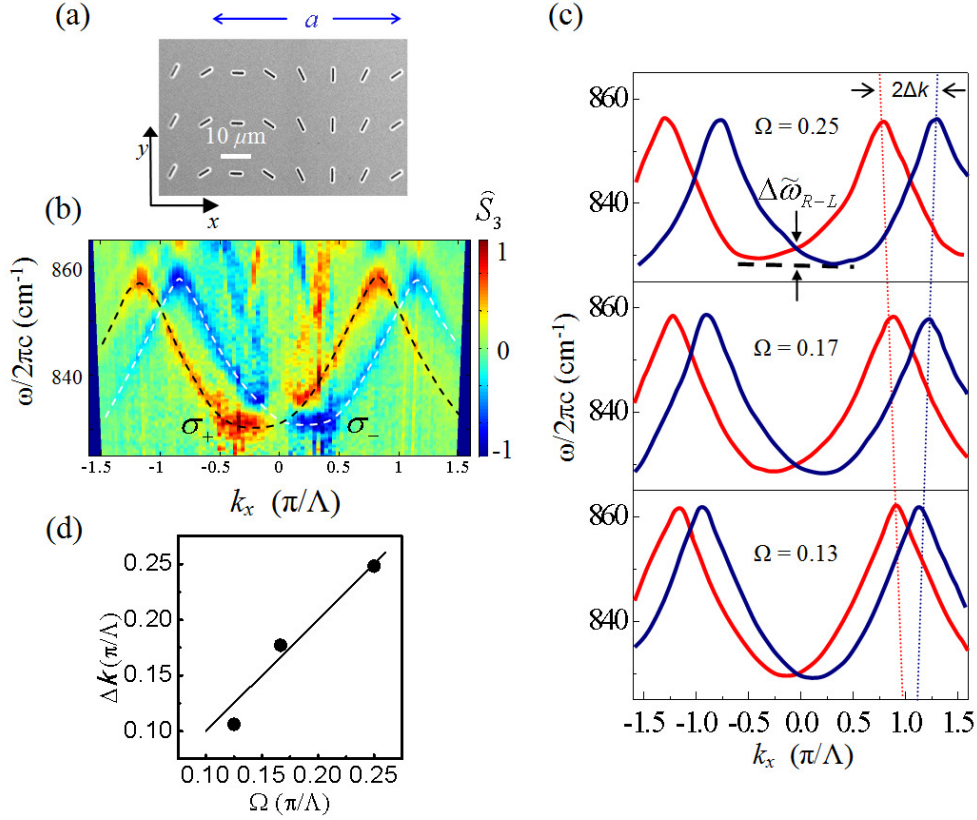
Fig. 5. (a) SEM of the L4 lattice composed of antennas rotating along the *x*-axis with spatial rotation rate $\Omega = 0.17\,(\pi / \Lambda)$. (b) Measured spin-projected dispersion of emission from L4 lattice obtained by the Stokes parameter S_3 measurement; blue/red color corresponds to a negative/positive spin projection. Dashed white and black lines highlight the spin split dispersion. (c) Measured spin-projected dispersion of the split $(0, \pm 1)$ modes for various Ω (in units of (π / Λ)); red and blue lines correspond to σ_+ and σ_- spin states, respectively; $\Delta \tilde{\omega}_{R-L}$ denotes the Rashba-like energy normalized by $\hbar / 2\pi c$. (d) Measured spin-controlled momentum displacement (circles), compared with the predicted dependence (solid line).

The peculiarity of the observed effect lies in its geometric nature. Surface waves scattered to radiation by a structure with spatially non-uniform anisotropy has a close analogy with emission from a revolving medium, as was recently shown [12]. Hence, the emission is most conveniently studied using a rotating reference frame that is attached to the axis of the local anisotropy of the antennas. The Helmholtz equation in a non-inertial reference frame revolving with rate $c\Omega << \omega$ is $(\nabla^2 + k^2 + 2\sigma\Omega k)E_\sigma = 0$, where E_σ are the eigenvectors of circular polarizations; note that $2\sigma\Omega k$ is the Coriolis term. This equation can be written as $(\nabla^2 + K^2)E_\sigma = 0$, where $K(\omega) \approx k(\omega) + \sigma\Omega$ is the generalized momentum, and the dispersion solution then becomes $\omega = \omega(k_x + \sigma\Omega)$. Therefore, due to rotation of the local anisotropy axis, the original dispersion of the homogeneous lattice is now split into two modes with opposite spin states, each shifted by $\Delta k = \sigma\Omega$ on the momentum axis as observed in our experiments (see Fig. 5(d)). The corresponding generalized momentum is the manifestation of the spin-orbit interaction, which is responsible for effects such as the optical

spin-Hall [20], Magnus, and Coriolis effects, and the Berry phase. The normalized Rashba Hamiltonian correction for the confined 1D system is $\tilde{H}_R = (2m^*/\hbar^2)H_R = 2m^*\alpha_R\sigma_y k_x/\hbar^2$, where σ_y is the Pauli spin operator [21]; note that in this case, the Schrödinger equation $(\nabla^2 + k^2 + 2m^*\alpha_R\sigma_y(-i\nabla)/\hbar^2)\Psi(x) = 0$ is similar to the Helmholtz equation in a revolving frame. The $\tilde{H}_R$ term corresponds to the Coriolis term $2\sigma\Omega k$, in accordance with our interpretation that Ω resembles $m^*\alpha_R/\hbar^2$.

We also investigated the dispersion of the inhomogeneous lattice (L4) along the k_y momentum direction and found non-split modes. The measured dispersion was identical to the cases involving a homogeneous lattice (L1 and L3), as expected from the homogeneity in the k_y direction for the L4 lattice. On the other hand, a spin split behavior was found for L4 in the 45° momentum direction, in agreement with the inversion asymmetry in this direction.

6. Conclusions

To conclude, we observed a spin-symmetry breaking of thermal radiation emitted from antenna lattices whose local anisotropy axis was sequentially rotated in space. The interaction between the SPhPs and the inhomogeneity of anisotropic structures results in a geometric correction to the dispersion of the scattered SPhPs. The correction of the dispersion relation is manifested by a spin-controlled momentum splitting of the radiation modes. Although our work focused on thermal emission applications, through the use of polar material (SiC), the same physics can be applied to any bulk material which supports surface waves. Our experiments pave the way for the manipulation of the photons' intrinsic degree of freedom in thermally excited emission, thus providing an important extension to the expanding field of *spinoptics*.

Acknowledgments